Journal of Metals, Materials and Minerals, 36(3), e2768, 2026

Effect of ZrO_2 content and oxide additives on the wear resistance of pressureless-sintered Si_3N_4 – ZrO_2 ceramic composites

Kamol TRAIPANYA[1], Thanakorn WASANAPIARNPONG[1,2,*] and Charusporn MONGKOLKACHIT[3]

[1] Department of Materials Science, Faculty of Science, Chulalongkorn University, Phyathai Road, Pathumwan, Bangkok 10330, Thailand
[2] Upcycled Materials from Industrial and Agricultural Wastes Research Unit, Department of Materials Science, Faculty of Science, Chulalongkorn University, Phyathai Road, Bangkok, 10330, Thailand
[3] National Metal and Materials Technology Center, National Science and Technology Development Agency, Khlong Luang, Pathumthani 12120, Thailand

***Corresponding author e-mail**: thanakorn.w@chula.ac.th

Received date:
3 June 2026
Revised date:
17 June 2026
Accepted date:
29 June 2026

Keywords:
Silicon nitride;
Zirconia;
Pressureless sintering;
Wear resistance;
Ceramic composites

Abstract

Silicon nitride (Si_3N_4) and zirconia (ZrO_2) ceramics are well-known for their excellent wear resistance, high hardness, and high mechanical strength. This research focuses on the development and investigation of Si_3N_4–ZrO_2 ceramic composites. Test specimens were fabricated by pressureless sintering at 1550°C to 1650°C for 2 h in a nitrogen atmosphere, using SiO_2, MgO, and Y_2O_3 as sintering additives. Density measurements indicated that the weight ratio of SiO_2:MgO:Y_2O_3 at 3:3:5 promoted densification and improved with the addition of ZrO_2 (3 mol% yttria-stabilized zirconia). However, the hardness of Si_3N_4 containing 5 wt% ZrO_2 was 14.63 GPa and showed a decreasing trend as the ZrO_2 content increased to 50 wt%. For the composite containing 75 wt% ZrO_2, the hardness dropped to 10.18 GPa when sintered at 1600°C. The flexural strength of sintered Si_3N_4 reached 924.42 MPa, which was comparable to that of pure ZrO_2 at 977.93 MPa. High-stress abrasion resistance testing according to ASTM B611 showed that the sample containing 5 wt% ZrO_2 exhibited the lowest volume loss of 18.97 mm^3. In comparison, pure Si_3N_4 showed a volume loss of 25.10 mm^3 under the same conditions, indicating that a small addition of 5 wt% ZrO_2 can enhance wear resistance. In contrast, the sample with 75 wt% ZrO_2 had the highest volume loss of 638.73 mm^3, while the 100 wt% ZrO_2 sample showed a loss of 543.74 mm^3. The results demonstrate that optimum wear resistance is achieved through a balance between zirconia content and liquid-phase stability rather than maximizing zirconia concentration.

1. Introduction

Tribological wear is one of the most critical challenges in industrial applications. Addressing this challenge is essential for enhancing the efficiency and durability of machinery, particularly in high-demand fields such as power generation and automotive industries. Such improvements are typically achieved by operating systems at higher speeds and minimizing friction losses. Consequently, the materials utilized must exhibit superior wear resistance. Silicon nitride (Si_3N_4) and zirconia (ZrO_2) ceramics are regarded as premier candidates for tribological applications due to their high mechanical strength and exceptional fracture toughness, both of which are critical for outstanding mechanical performance [1–4].

As high-performance materials, sintered silicon nitride ceramics are frequently employed in demanding structural applications that require high strength, stiffness, thermal stability, low coefficients of friction, and high wear resistance. Achieving these properties relies heavily on the sintering process. However, the densification of pure Si_3N_4 is inherently challenging due to its high-temperature volatility and low lattice diffusivity arising from strong covalent bonding; these characteristics tend to cause microstructure coarsening and oxidation rather than densification [5]. Consequently, liquid-phase sintering is required, necessitating the addition of sintering aids such as Y_2O_3, MgO, and Al_2O_3 . These additives react with the native SiO_2 layer on the Si_3N_4 particles to form an oxynitride liquid phase, which promotes densification through particle rearrangement and dissolution-precipitation mechanisms [6,7].

Zirconia is another crucial ceramic material owing to its unique chemical and physical properties, including ionic conductivity, low thermal conductivity, high hardness, and low friction [8]. Zirconia is distinguished by its polymorphic nature, existing in monoclinic, tetragonal, and cubic phases. The martensitic phase transformation from tetragonal to monoclinic upon cooling is particularly significant. This transformation is accompanied by a substantial volume expansion of approximately 4% to 5% and a shear strain of roughly 0.16 [9]. While unconstrained expansion leads to catastrophic material failure, alloying with stabilizing oxides (such as MgO, Y_2O_3, CeO_2) allows the tetragonal phase to be retained in a metastable state at room temperature [8]. When incorporated as a secondary phase in ceramic matrices (such as alumina or silicon nitride), this metastable tetragonal phase can undergo stress-induced transformation to provide transformation toughening. In contrast, existing literature often focuses on reinforcing

Si_3N_4 matrices with other nitrides or carbides to optimize the mechanical and functional properties of the resulting composites.

In tribological contexts, the sliding of Si_3N_4 against high-temperature alloys exhibits varying friction coefficients and wear rates, largely dictated by the formation of protective oxide tribo-layers [10]. Utilizing the complementary advantages of both Si_3N_4 and ZrO_2, previous studies have successfully developed high-density, high-strength Si_3N_4–ZrO_2 composite [11]. However, while the fabrication of dense Si_3N_4–ZrO_2 composites has been reported, the combined influence of zirconia content and liquid-phase additive concentration on high-stress abrasion resistance remains poorly understood. Therefore, this study aims to systematically investigate the effect of ZrO_2 content and sintering additive ratios on the densification, mechanical properties, and specifically, the high-stress abrasion behavior of Si_3N_4–ZrO_2 ceramic composites.

2. Materials and experimental

The raw materials used in this study consisted of high-purity α-Si_3N_4 powder (SN E-10 grade, Ube Industries Ltd., Tokyo, Japan) and 3 mol% Y_2O_3-stabilized ZrO_2 powder (Inframat Advanced Materials). The ZrO_2 was added at concentrations of 5 wt%, 25 wt%, 50 wt%, and 75 wt%. Additionally, SiO_2 (KE-P30, Nippon Shokubai Co. Ltd., Osaka, Japan), MgO (MJ-30, Iwatani Corp., Tokyo, Japan), and Y_2O_3 (RU, Shin-Etsu Chemical Co. Ltd., Tokyo, Japan) were used as sintering additives. The weight ratio of the SiO_2 : MgO : Y_2O_3 additives were kept at 3 : 3 : 5 for the constant-additive series (Zr series) and the reduced-additive series (ZrA series) for proportional reduction in additive concentration with increasing ZrO_2 content, as detailed in Table 1.

Table 1. Chemical compositions of Si_3N_4–ZrO_2 composites with constant-additive (Zr) and reduced-additive (ZrA) systems (wt%).

Composition	SN	5Zr	25Zr	50Zr	75Zr	5ZrA	25ZrA	50ZrA	75ZrA	Zr
Si_3N_4	89	84	64	39	14	84.55	67.85	45.05	22.25	-
MgO	3	3	3	3	3	2.85	1.95	1.35	0.75	-
SiO_2	3	3	3	3	3	2.85	1.95	1.35	0.75	-
Y_2O_3	5	5	5	5	5	4.75	3.25	2.25	1.25	-
ZrO_2	-	5	25	50	75	5	25	50	75	100
Total	**100**	**100**	**100**	**100**	**100**	**100**	**100**	**100**	**100**	**100**

Table 2. Bulk density, relative density, water absorption, and apparent porosity of Si_3N_4–ZrO_2 composites sintered at 1550°C to 1650°C for 2 h in a nitrogen atmosphere.

Samples	Bulk density [g·cm^{-3}]	Relative density [%]	Water absorption [%]	Apparent porosity [%]
SN - 1650	3.21	99.32	0.03	0.10
SN - 1600	3.19	98.82	0.08	0.25
SN - 1550	3.08	95.46	0.03	0.09
5Zr - 1650	3.29	99.45	0.05	0.16
5Zr- 1600	3.26	98.57	0.09	0.28
5Zr - 1550	3.25	98.32	0.01	0.05
25Zr - 1650	3.64	99.25	0.04	0.13
25Zr - 1600	3.64	99.28	0.04	0.15
25Zr - 1550	3.65	99.53	0.05	0.19
50Zr - 1650	4.19	98.80	0.03	0.13
50Zr - 1600	4.21	99.23	0.12	0.52
50Zr - 1550	4.19	98.87	0.06	0.26
75Zr - 1650	4.72	93.71	0.55	2.55
75Zr - 1600	4.94	98.14	0.05	0.27
75Zr - 1550	4.99	99.22	0.16	0.78
5ZrA - 1650	3.28	99.19	0.24	0.79
5ZrA - 1600	3.25	98.47	0.21	0.67
5ZrA - 1550	3.22	97.44	0.07	0.22
25ZrA - 1650	3.62	99.01	0.08	0.29
25ZrA - 1600	3.60	98.68	0.03	0.10
25ZrA - 1550	3.60	98.59	0.13	0.47
50ZrA - 1650	4.18	99.20	0.13	0.56
50ZrA - 1600	4.17	98.82	0.05	0.20
50ZrA - 1550	4.14	98.27	0.13	0.55
75ZrA - 1650	4.88	97.89	0.08	0.38
75ZrA - 1600	4.84	97.02	0.02	0.08
75ZrA - 1550	4.84	96.95	0.04	0.17
Zr - 1650	6.05	99.18	0.03	0.18
Zr - 1600	6.06	99.32	0.07	0.42
Zr - 1550	6.08	99.72	0.14	0.88

In the Zr series, the sintering additive level was held constant regardless of zirconia content, resulting in an approximately constant liquid-phase fraction during sintering. Conversely, in the ZrA series, the additive level was reduced in proportion to the ZrO_2 content, yielding a systematically decreasing liquid-phase fraction with increasing ZrO_2 addition. Then the starting material powders were mixed by ball milling in a high-density polyethylene bottle (HDPE) with Si_3N_4 ball in 99.9% ethanol for 24 h. The slurry was dried to powder in a rotary evaporator at 60°C through a 100-mesh screening sieve. The samples were prepared with dimensions of 15 mm × 60 mm × 5 mm by uniaxial pressing at 25 MPa, followed by cold isostatic pressing at 250 MPa for 5 min. The samples were sintered at 1550°C, 1600°C, and 1650°C for 2 h in a nitrogen atmosphere of 0.1 MPa using Hi-Multi 5000 furnace (Fujidempa Kogyo, Japan).

Phase identification of the samples sintered at 1650°C was performed by X-ray diffraction (XRD) using Cu-Kα radiation (λ = 1.54 Å) in the 2-theta range of 10° to 80°. The bulk density, water absorption, and apparent porosity were determined by the Archimedes method according to ASTM C373-16. For mechanical testing, the sintered materials were ground and polished. Vickers hardness was evaluated under a load of 10 kgf for 15 s, averaged over 10 indentations. Fracture toughness was evaluated using the Vickers indentation technique by measuring the crack length and estimating the value based on the Evans and Charles theory [12]. Flexural strength was determined via the three-point bending method with a span length of 30 mm using 5 specimens. For microstructural analysis, all samples were polished down to a 1 μm diamond finish and thermally etched at 1550°C for 15 min in a nitrogen atmosphere furnace prior to scanning electron microscopy (SEM) observation. Finally, the wear resistance of 3 specimens was evaluated by custom-built apparatus in accordance with the ASTM B611-13 standard for high-stress abrasion resistance.

3. Results and discussion

3.1 Densification behavior and physical properties

From Table 2, the densification behavior of the Si_3N_4–ZrO_2 ceramic composites is primarily influenced by the zirconia content, sintering additive concentration, and sintering temperature. The incorporation of ZrO_2 into the Si_3N_4 matrix increased the bulk density across all sintering temperatures. The Si_3N_4 samples (SN series) exhibited bulk densities ranging from 3.08 $g \cdot cm^{-3}$ to 3.21 $g \cdot cm^{-3}$, whereas the monolithic ZrO_2 samples (Zr series) exceeded 6.00 $g \cdot cm^{-3}$. This density increase follows the rule of mixtures, attributed to the significantly higher theoretical density of zirconia compared to silicon nitride.

Because silicon nitride is a strongly covalent material, solid-state sintering is thermodynamically unfavorable. Consequently, densification primarily relies on liquid-phase sintering promoted by MgO, SiO_2, and Y_2O_3 additives [11,13]. At elevated temperatures, these oxides react with the native silica layer on the Si_3N_4 particle surfaces to form a transient oxynitride liquid phase, which enhances particle rearrangement and solution–precipitation mechanisms. For the baseline compositions, particularly the SN and low-Zr samples, increasing the sintering temperature from 1550°C to 1650°C generally enhanced densification.

At 1550°C, the liquid phase likely possessed a relatively high viscosity, which restricted efficient particle rearrangement and mass transport. Elevating the sintering temperature to 1600°C and 1650°C reduced the liquid-phase viscosity, thereby facilitating near-theoretical densification (>99% relative density) and minimizing apparent porosity.

A significant difference was observed between the constant-additive series (Zr series) and the reduced-additive series (ZrA series). In the Zr series, the fixed amount of sintering additives maintained a relatively stable volume of the liquid phase regardless of the zirconia content. In contrast, the ZrA series employed a proportional reduction in additive concentration with increasing ZrO_2 content. For instance, in the 75ZrA composition, the Y_2O_3 content decreased to 1.25 wt%, while the MgO and SiO_2 contents were reduced to 0.75 wt% each. This lower availability of liquid-phase-forming additives restricted mass transport during sintering, resulting in lower relative densities and increased water absorption compared to the corresponding Zr series samples.

Sintering could not proceed efficiently without a sufficient volume of the intergranular glassy phase [13]. In particular, the 75Zr sample sintered at 1650°C showed a noticeable decrease in relative density to 93.71%, accompanied by an increase in apparent porosity to 2.55%. Although higher temperatures generally promote densification, this observed decrease in density may indicate over-firing effects associated with the evaporation of glassy phases [14]. At excessively high temperatures, volatilization of glassy-phase constituents and gas evolution may occur, particularly in compositions containing high zirconia contents, resulting in residual porosity and microstructural degradation [15,16].

3.2 Mechanical and tribological properties

Figure 1 presents the flexural strength of the sintered samples at 1550°C, 1600°C, and 1650°C. The SN samples sintered at 1600°C demonstrated a maximum flexural strength exceeding 900 MPa, which is attributed to the reconstructive phase transformation from α-Si_3N_4 to β-Si_3N_4. The unidirectional growth mechanism of the β-phase produces an interlocked, acicular grain structure that inherently reinforces the matrix against applied bending moments [2,17]. However, the introduction of zirconia led to a decrease in flexural strength. The 5Zr, 25Zr, and 50Zr samples exhibited strengths fluctuating between 400 MPa and 600 MPa, which are significantly lower than those of the SN samples. This strength deficit indicates the effects of structural anisotropy and thermal mismatch. The coefficient of thermal expansion (CTE) of ZrO_2 is significantly higher than that of Si_3N_4 [18]. During the cooling cycle, the dispersed zirconia particles contract more than the surrounding rigid silicon nitride matrix. Because these disparate materials are rigidly bonded via the intergranular boundary glass, this differential shrinkage generates radial tensile and tangential compressive stresses across the interphase boundaries [19]. These residual stresses act additively with external loads, effectively lowering the critical threshold of applied stress required to initiate intergranular fracture. The most severe mechanical degradation occurred in the 75Zr samples, where the flexural strength dropped below 100 MPa across all sintering temperatures. For the ZrA series, the flexural strength of the samples with reduced additives highlights the criticality of the liquid phase. The sharp drop in flexural strength observed in the 75ZrA sample, as well as the generally lower strengths of 25ZrA and 50ZrA compared to the SN samples, is not solely due to phase transformation, but also

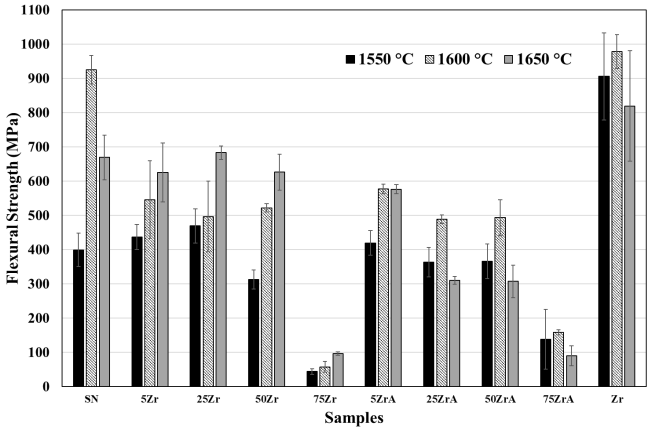

Figure 1. Effect of ZrO_2 content and sintering temperature on the flexural strength of Si_3N_4–ZrO_2 composites.

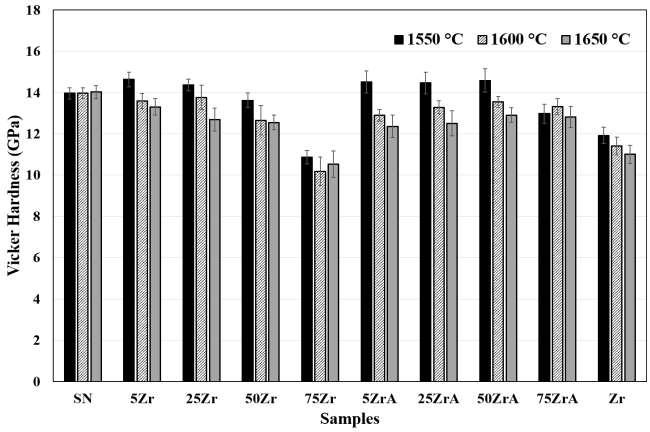

Figure 2. Vickers hardness of Si_3N_4–ZrO_2 composites as a function of ZrO_2 content and sintering temperature.

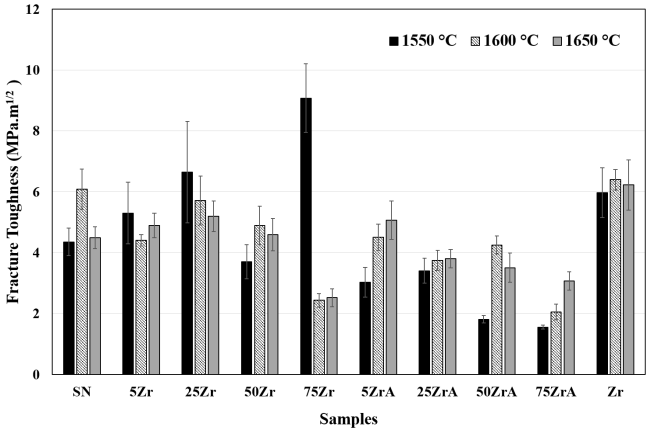

Figure 3. Fracture toughness of Si_3N_4–ZrO_2 composites sintered at different temperatures.

to residual porosity. The lower volume of liquid phase in the ZrA series failed to facilitate adequate mass transport to eliminate interconnected pores during sintering, as confirmed by the SEM microstructures.

The fracture toughness of the SN samples exhibits stable values ranging from approximately 4.5 MPa·$m^{1/2}$to 6.0 MPa·$m^{1/2}$, deriving energy absorption strictly from crack-wake bridging and crack deflection provided by the elongated grains. When 5 wt% and 25 wt% zirconia was introduced, the fracture toughness fluctuated but remained viable. In these specific configurations, assuming adequate densification, the classical transformation toughening mechanism was actively engaged. The stress field of an advancing crack triggers a highly localized, stress-induced martensitic transformation of the well-constrained tetragonal zirconia particles located directly within the frontal process zone [10]. The resulting compressive stress effectively shields the crack tip, increasing the total thermodynamic energy required to drive the fracture surface forward.

However, an anomaly occurred in the 75Zr sample sintered at 1550°C, where the fracture toughness increased drastically to approximately 9.0 MPa·$m^{1/2}$. While numerically impressive, this spike does not represent the intrinsic fracture toughness of the material, as evidenced by its extremely low flexural strength. In the 75Zr sample, extensive microcracking artificially inflated the measured toughness values. Because the sample was already severely ruptured by spontaneous and unconstrained phase expansion during cooling, the propagation of an induced crack caused the primary fissure to continuously branch and bifurcate into the pre-existing microcrack network [20]. Although this massive crack branching absorbed significant fracture energy during testing, the specimen itself was already structurally compromised. At higher sintering temperatures (1600°C and 1650°C), the toughness of the 75Zr sample dropped back to 2.5 MPa·$m^{1/2}$, indicating that elevated temperatures promoted detrimental grain growth and boundary phase volatilization.

Figure 4 illustrates the wear resistance of all sintered samples. The data plot demonstrates that the wear resistance of the Si_3N_4–ZrO_2 composites is not solely a function of the zirconia weight fraction but is strongly governed by the stability of the intergranular glassy phases generated during liquid-phase sintering. The SN samples and the 5 wt% zirconia (5Zr) composite maintained excellent structural integrity when sintered at 1550°C and 1600°C, registering volumetric wear losses below 50 cm^3. However, a distinct structural vulnerability emerged when the sintering temperature was elevated to 1650°C, where both the SN and 5Zr samples experienced a sharp increase in volumetric degradation. This high-temperature degradation is attributed to boundary phase volatilization. During liquid-phase sintering, oxide additives (Y_2O_3, MgO, and SiO_2) react to form an oxynitride glassy phase at the grain boundaries, which is essential for sample densification [21].

At 1650°C, the vapor pressure of these volatile oxide constituents increases significantly, leading to localized evaporation of the glassy phase and the subsequent generation of secondary intergranular porosity. Under abrasive sliding stresses, this weakened intergranular cohesion allows cracks to propagate easily, bypassing the intrinsic hardness of the constituent grains and resulting in elevated macroscopic wear [22].

In the standard baseline composites (ranging from SN to 75Zr), the total content of oxide sintering additives is held strictly constant at 11 wt% (3 wt% MgO + 3 wt% SiO_2 + 5 wt% Y_2O_3), regardless of the volumetric displacement of the primary matrix by the zirconia inclusions. Conversely, the "A" series implements a proportional reduction approach, wherein the absolute mass of the liquid-phase-forming oxides is systematically decreased in direct stoichiometric proportion to the reduction of the primary silicon nitride phase. This compositional shift alters the intergranular film thickness and the thermal stability of the glassy boundary phases, thereby dictating the tribological endurance of the composites under load [23].

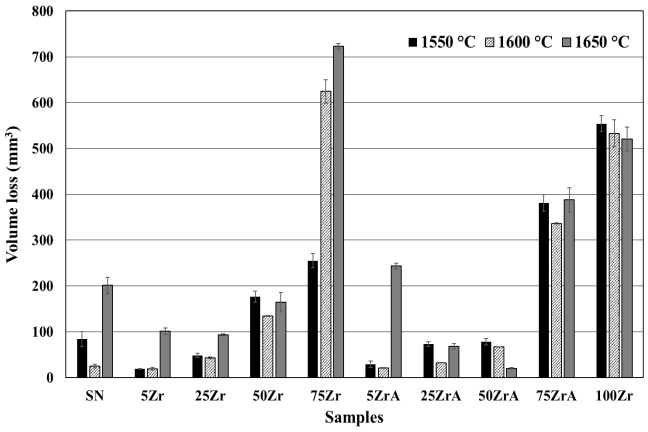

Figure. 4 Volume loss of Si_3N_4–ZrO_2 composites after high-stress abrasion testing (ASTM B611) as a function of sintering temperature.

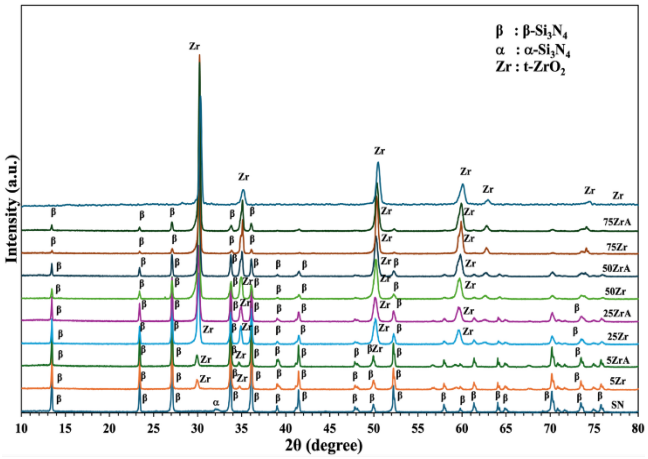

Figure. 5 XRD patterns of Si_3N_4–ZrO_2 composites sintered at 1650°C showing β-Si_3N_4 and tetragonal ZrO_2 phases.

An anomalous degradation was observed in the 5ZrA formulation at the elevated sintering temperature of 1600°C. At a 5 wt% zirconia content, in the "A" series reduced the total additive package from the baseline 11 wt% down to 10.45 wt% (2.85 wt% + 2.85 wt% + 4.75 wt%). While this minor reduction provided a sufficient volume of eutectic silicate liquid for adequate capillary densification at 1550°C and 1600°C, it subtly altered the precise stoichiometry and localized networking of the resulting oxynitride intergranular glass.

Upon sintering at 1650°C, the modified boundary phase crosses a critical volatility threshold. The higher temperature may promote volatilization of the liquid-phase constituents, leading to increased porosity and reduced wear resistance [22]. During abrasive sliding contact, these volatile-depleted and weakened interphase boundaries could not support the compressive and shear loads induced by the test. This localized structural deficiency led directly to rapid intergranular fracture, accelerating the volumetric wear loss to approximately 240 cm^3 exclusively at 1650°C.

For the 50ZrA composite, which demonstrates an inverse relationship between sintering temperature and tribological wear loss. The explicit compositional data indicates that the 50ZrA formulation the additives was reduced to 4.95 wt% (1.35 wt% SiO_2 + 1.35 wt% MgO + 2.25 wt% Y_2O_3), compared to the 11 wt% excess presents in the standard 50Zr formulation. At conventional sintering temperatures (1550°C and 1600°C), this insufficient additive content resulted in deficient phase boundaries that fractured and wore rapidly under tribological loads. However, when the sintering temperature was raised to 1650°C, the lower viscosity of the liquid phase allowed the melt to efficiently wet and infiltrate the ZrO_2 and Si_3N_4 grain boundaries. Because the volume of the glassy phase was restricted by the initial 4.95 wt% composition, the resulting microstructure featured thin, structurally robust intergranular films, effectively eliminating the thick, mechanically weak glassy pockets observed in the standard 50Zr composite. Consequently, the 50ZrA composite sintered at 1650°C successfully utilized the stress-induced phase transformation of zirconia without boundary failure, achieving a minimal wear loss of approximately 20 cm^3. Finally, for the 75ZrA composite, the total additive content dropped to 2.75 wt%. This severe deficiency led to incomplete densification via pressureless sintering, reducing its relative density and resulting in a high wear volume loss ranging from 340 cm^3 to 390 cm^3.

3.3 Phase evolution and crystalline structure

Figure 5 illustrates the XRD patterns of the SN, Zr, and both the standard and "A" series Si_3N_4–ZrO_2 composite samples sintered at 1650°C. The monolithic Si_3N_4 (SN) sample, prepared with SiO_2, MgO, and Y_2O_3 as sintering additives, exhibits β-Si_3N_4 as the predominant crystalline phase. Since the eutectic temperature of the SiO_2-MgO-Y_2O_3 system is approximately 1400°C, effective liquid-phase sintering was successfully achieved at 1650°C without the need for powder bed packing [13,24]. For the composite samples, the XRD diffractograms are characterized exclusively by β-Si_3N_4 and tetragonal zirconia (t-ZrO_2) phase. At lower zirconia contents (5Zr and 5ZrA), the diffraction patterns are dominated by sharp, high-intensity peaks corresponding to the β-Si_3N_4 phase. The complete absence of residual α-Si_3N_4 peaks demonstrates that the selected oxide additive packages-even at the reduced concentrations in the "A" series–were sufficient to form the eutectic silicate liquid required to drive the complete α-Si_3N_4 to β-Si_3N_4 phase transformation.

Furthermore, as the zirconia composition increases from 5 wt% up to 75 wt%, the diffraction peaks corresponding to the tetragonal zirconia structure become progressively more pronounced. Crucially, no distinct crystallographic evidence of the monoclinic zirconia (ZrO_2) phase was detected in any of the sintered bulk materials. This indicates that the Y_2O_3 constituent within the sintering additives successfully partitioned and alloyed into the zirconia lattice, effectively stabilizing the tetragonal phase at room temperature. Nevertheless, correlating this XRD data with the previously discussed mechanical and tribological properties helps elucidate the structural failure observed in the "A" series composites. The XRD pattern for the 75ZrA formulation confirms the retention of the tetragonal zirconia phase, despite this specific composition suffering from an inadequate volume of liquid phase during sintering due to its low Y_2O_3 content (1.25 wt%). Consequently, while the 75ZrA sample theoretically retains the capacity for stress-induced transformation toughening (as proven by the presence of the tetragonal phase), its mechanical performance is severely compromised because the severe deficiency in sintering additives leaves the grain boundaries structurally weak and highly porous.

3.4 Microstructural characterization

Figure 6–7 illustrate the scanning electron micrographs (SEM) of the sintered samples. The microstructural features are closely correlated with the chemical compositions (Table 1) and the volumetric wear loss (Figure 4), revealing a profound link between bulk density (Table 2) and microstructural morphology. The SEM images of the 5 wt% zirconia (5Zr) composite in Figure 6(d-f) display highly dense, equiaxed zirconia particles (brighter phase) embedded within a network of elongated β-Si_3N_4 (hexagonal rod-like) grains. This dense microstructure was facilitated by the constant 11 wt% sintering additive package, corresponding to the high hardness (14.5 GPa) and fracture toughness (5.3 MPa.$m^{1/2}$) obtained at 1550°C.

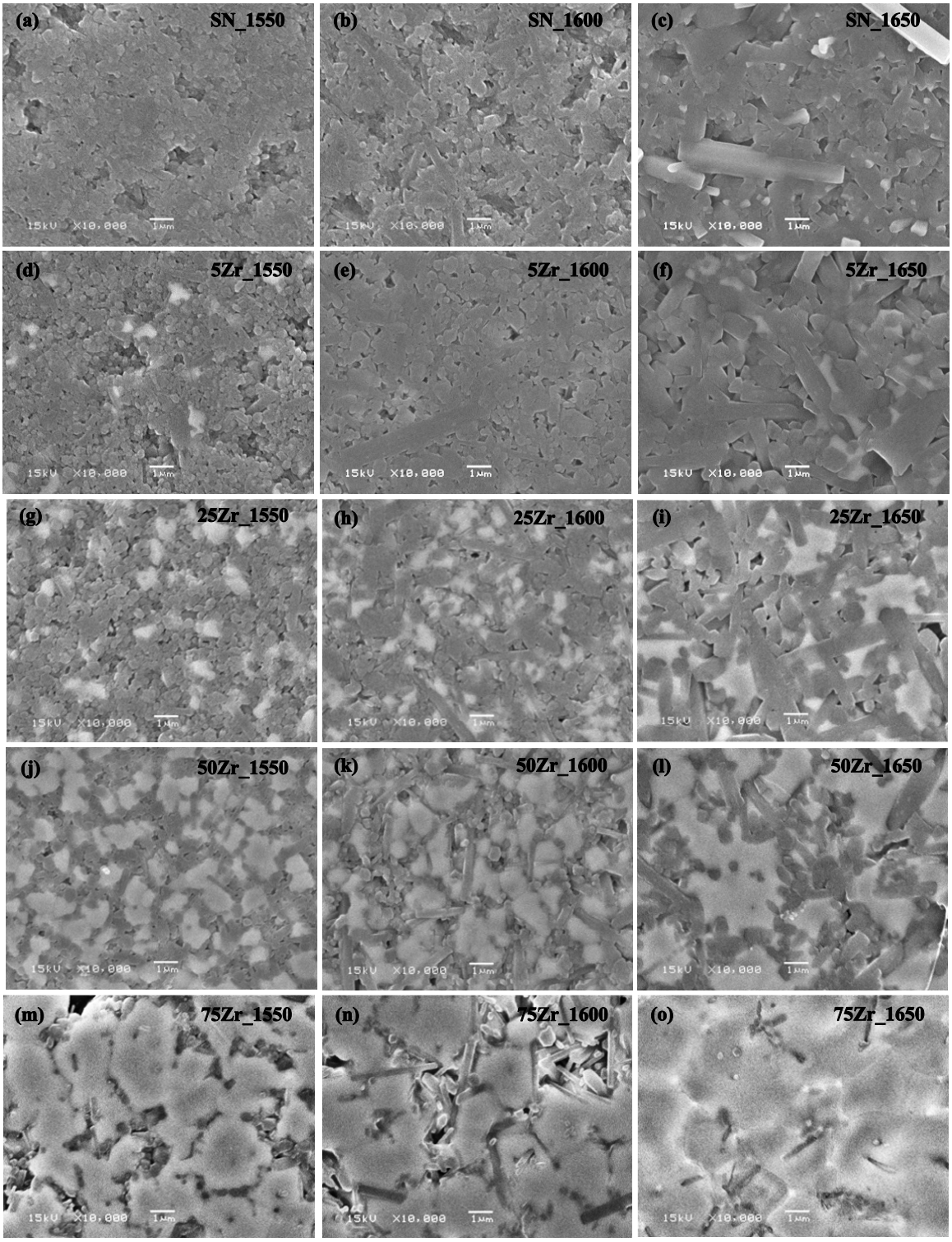

Figure 6. SEM micrographs of the constant-additive Si_3N_4–ZrO_2 composites (Zr series) sintered at 1550°C to 1650°C: (a–c) SN, (d–f) 5Zr, (g–i) 25Zr, (j–l) 50Zr, and (m–o) 75Zr.

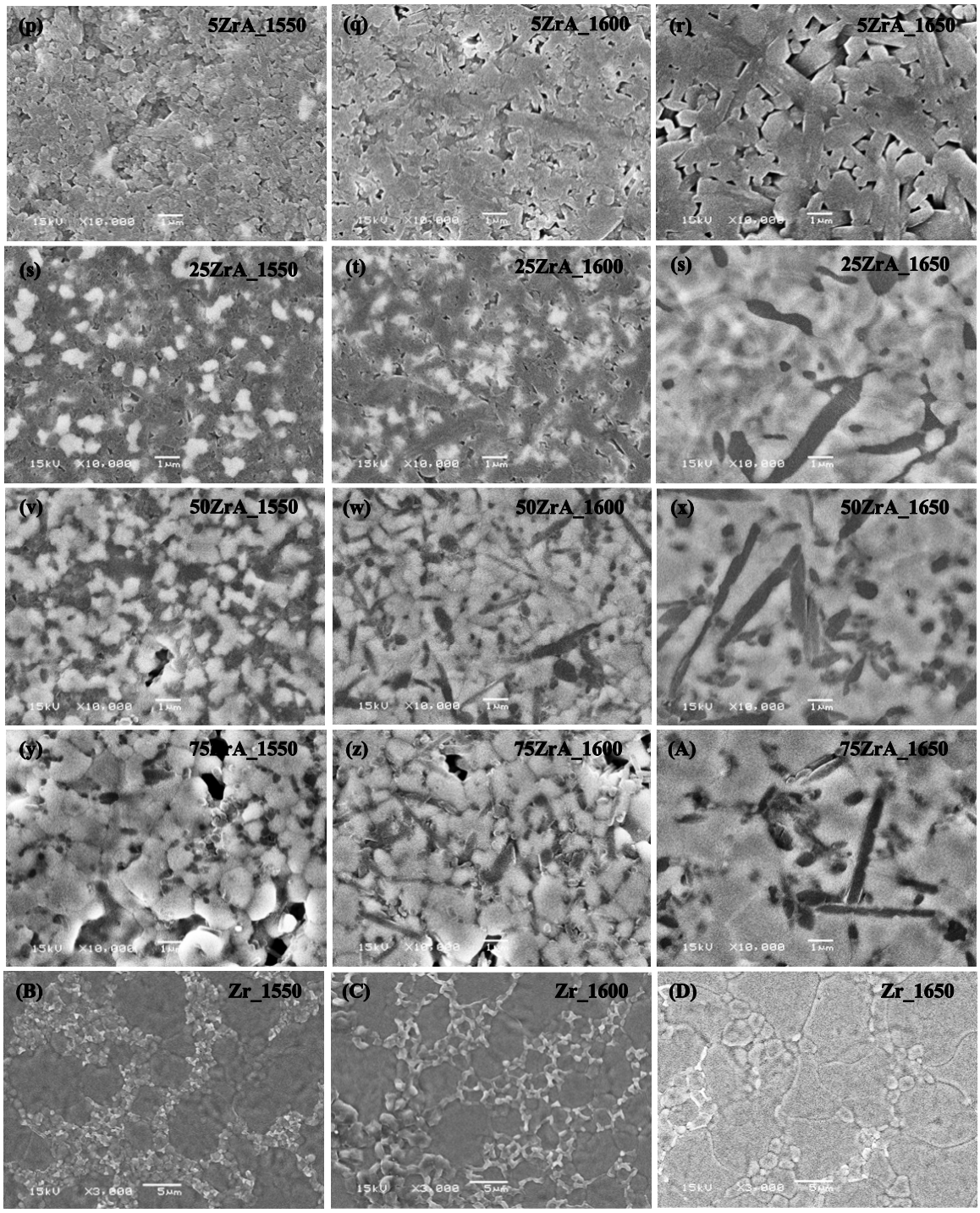

Figure 7. SEM micrographs of the reduced-additive Si_3N_4–ZrO_2 composites (ZrA series) and monolithic ZrO_2 samples sintered at 1550°C to 1650°C: (p–r) 5ZrA, (s–u) 25ZrA, (v–x) 50ZrA, (y–A) 75ZrA, and (B–D) ZrO_2.

In contrast, the "A" series generates distinct microstructural variations. The 50ZrA samples in Figure 7(v-x) clearly show the distribution of zirconia within the matrix, where higher sintering temperatures (1600°C and 1650°C) induced grain growth; nevertheless, this composition exhibited exceptional wear resistance when sintered at 1650°C. Conversely, the 5ZrA samples suffered from the detrimental effects of boundary phase volatilization at 1650°C due to their subtly altered additive stoichiometry, which created intergranular porosity and microstructural defects that led to severe abrasive wear loss.

Finally, the poor performance of the 75 wt% zirconia samples (75Zr and 75ZrA) is primarily attributed to a severe deficiency in the liquid phase and chemical instability. As indicated in the composition table, the 75ZrA formulation contains an insufficient total additive content of only 2.75 wt%, with just 1.25 wt% of Y_2O_3 stabilizer, which falls far below the threshold required for effective liquid-phase sintering. Consequently, the SEM images reveal a highly porous and fragmented microstructure dominated by large zirconia agglomerates, lacking a continuous silicon nitride skeleton to reinforce the matrix. Without

sufficient intergranular bonding and compounded by the internal stresses induced during the unconstrained zirconia phase transformation, the material degraded rapidly under sliding contact, leading to severe grain pull-out. This structural failure directly accounts for the extremely high wear volume loss of 600 mm^3 to 720 mm^3 recorded in the wear analysis.

4. Conclusions

This study investigated the densification, mechanical properties, and wear resistance of Si_3N_4–ZrO_2 ceramic composites prepared via pressureless sintering at 1550°C, 1600°C, and 1650°C, focusing on the effects of ZrO_2 content (5 wt% to 75 wt%) and two sintering additive systems: a constant additive package (Zr series) and a proportionally reduced additive package (ZrA series). The key findings can be summarized as follows:

1) Densification Behavior: Most compositions achieved high relative densities (>98%) when sintered at 1600°C. However, the 75Zr sample sintered at 1650°C exhibited a significant density drop to 93.71% due to over-firing and the subsequent volatilization of the intergranular glassy phase. Furthermore, the ZrA series with high ZrO_2 content suffered from an insufficient liquid phase, which restricted mass transport and led to incomplete densification.

2) Mechanical Properties: The monolithic Si_3N_4 (SN) sample sintered at 1600°C achieved the highest flexural strength of approximately 924 MPa, which is attributed to the interlocking of the acicular β-Si_3N_4 grain structure. The introduction of ZrO_2 generally degraded the flexural strength due to thermal expansion mismatch, with the 75Zr samples exhibiting the lowest strengths (<100 MPa) across all temperatures. Vickers' hardness peaked at ~14.5 GPa for 5Zr sample at 1550°C and declined to ~10 GPa at 75 wt% ZrO_2. While the fracture toughness of the SN samples ranged from 4.5 $MPa \cdot m^{1/2}$ to 6.0 $MPa \cdot m^{1/2}$, an anomalously high toughness of ~9.0 $MPa \cdot m^{1/2}$ was observed in the 75Zr sample sintered at 1550°C; this spike was attributed to microcrack-induced artificial inflation rather than true intrinsic toughness.

3) Wear Resistance: The 5Zr composite demonstrated the highest wear resistance, exhibiting the lowest volumetric wear loss of ~18.97 mm^3, outperforming the monolithic SN sample (~25.10 mm^3). Notably, the 50ZrA sample sintered at 1650°C also performed exceptionally well (~20 mm^3) due to the formation of thin, structurally robust inter-granular films derived from the restricted additive content. Conversely, the 75ZrA composite exhibited the poorest tribological performance (600 mm^3 to 720 mm^3) due to severe liquid-phase deficiency, stabilized zirconia phase transformation stresses, and a highly porous, fragmented microstructure.

Ultimately, optimal wear resistance in Si_3N_4–ZrO_2 composites is achieved not by simply maximizing the ZrO_2 content, but by precisely balancing the additive concentration, sintering temperature, and inter-granular microstructural integrity.

References

[1] M. Liu, and S. Chen, "Micromechanical characterization of zirconia and silicon nitride ceramics using indentation and scratch methods," *Ceramics International*, vol. 50, no. 11 part B, pp. 19982–20010, 2024.

[2] F. L. Riley, "Silicon nitride and related materials," *Journal of the American Ceramic Society*, vol. 83, no. 2, pp. 245–265, 2000.

[3] Z. Krstic, and V. D. Krstic, "Silicon nitride: the engineering material of the future," *Journal of Materials Science*, vol. 47, pp. 535–552, 2012.

[4] A. Leriche, F. Cambier, and H. Reveron, "Zirconia ceramics, structure and properties," *Encyclopedia of materials: technical ceramics and glasses*, vol. 2, pp. 93–104, 2021.

[5] C. Greskovich, S. Prochazka, and J. H. Rosolowski, "Sintering behavior of covalently-bonded materials," *Nitrogen Ceramics*, pp. 351–357, 1977.

[6] K. Jeong, J. Tatami, M. Iijima, and T. Nishimura, "Spark plasma sintering of silicon nitride using nanocomposite particles," *Advanced Powder Technology*, vol. 28, no. 1, pp. 37–42, 2017.

[7] S. Chockalingam, and D. A. Earl, "Microwave sintering of Si_3N_4 with $LiYO_2$ and ZrO_2 as sintering additives", *Materials & Design*, vol. 31, no. 3, pp. 1559–1562, 2010.

[8] R. H. J. Hannink, P. M. Kelly, and B. C. Muddle, "Transformation toughening in zirconia-containing ceramics," *Journal of the American Ceramic Society*, vol. 83, no. 3, pp. 461–487, 2000.

[9] R. C. Garvie, R. H. Hannink, and R. T. Pascoe, "Ceramic steel?," *Nature*, vol. 258, pp. 703–704, 1975.

[10] C. Huang B. Zou, Y. Liu, S. Zhang, C. Huang, and S. Li, "Study on friction characterization and wear-resistance properties of Si_3N_4 ceramic sliding against different high-temperature alloys," *Ceramics International*, vol. 42, no. 15, pp. 17210–17221, 2016.

[11] K. Traipanya, T. Wasanapiarnpong, and C. Mongkolkachit, "Fabrication and characterizations of high density Si_3N_4 - ZrO_2 ceramics," *Journal of Metals, Materials and Minerals*, vol. 33, no. 3, p. 1621, 2023.

[12] A. G. Evans, and E. A. Charles, "Fracture toughness determinations by indentation," *Journal of the American Ceramic Society*, vol. 59, no. 7–8, pp. 371–372, 1976.

[13] T. Wasanapiarnpong, S. Wada, M. Imai, and T. Yano, "Lower temperature pressureless sintering of Si_3N_4 ceramics using SiO_2-MgO-Y_2O_3 additives without packing powder," *Journal of the Ceramic Society of Japan*, vol. 114, pp. 733–738, 2006.

[14] T. Wasanapiarnpong, S. Wada, M. Imai, and T. Yano, "Effect of post-sintering heat-treatment on thermal and mechanical properties of Si_3N_4 ceramics sintered with different additives," *Journal of the European Ceramic Society*, vol. 26, no. 15, pp. 3467–3475, 2006.

[15] F. F. Lange, "Silicon nitride polyphase systems: fabrication, microstructure, and properties," *International Metals Reviews*, vol. 25, no. 1, pp. 1–20, 1980.

[16] F. F. Lange, "Volatilization associated with the sintering of polyphase Si_3N_4 materials," *Journal of the American Ceramic Society*, vol. 65, pp. 1982.

[17] P. F. Becher, "Microstructural design of toughened ceramics," *Journal of the American Ceramic Society*, vol. 74, no. 2, pp. 255–269, 1991.

[18] J. J. Kruzic, R. M. Cannon, and R. O. Ritchie, "Effects of moisture on grain-boundary strength, fracture, and fatigue properties of alumina", *Journal of the American Ceramic Society*, vol. 88, no. 8, pp. 2236–2245, 2005.

[19] C. Greskovich, and J. H. Rosolowski, "Sintering of covalent solids," *Journal of the American Ceramic Society*, vol. 59, no. 7–8, pp. 336–343, 1976.

[20] W. E. Lee, and W. M. Rainforth, "*Ceramic Microstructures : Property control by processing*," Springer Dordrecht, 1994. page 590.

[21] M. H. Bocanegra-Bernal, and B. Matovic, "Dense and near-net-shape fabrication of Si_3N_4 ceramics," *Materials Science and Engineering: A*, vol. 500, pp. 130–149, 2009.

[22] S. Hampshire, "Oxynitride glasses, their properties and crystallisation – a review," *Journal of Non-Crystalline Solids*, vol. 316, no. 1, pp. 64–73, 2003.

[23] H. J. Kleebe, "Structure and chemistry of interfaces in Si_3N_4 ceramics studied by transmission electron microscopy," *Journal of the Ceramic Society of Japan*, vol. 105, pp. 453–475, 1997.

[24] S. Kuang, M. Hoffmann, H. L. Lukas, and G. Petzow, "Experimental study and thermodynamic calculations of the MgO-Y_2O_3-SiO_2 system," *Key Engineering Materials*, vol. 89–91, pp. 399–404, 1993.